IOP Publishing Multifunct. Mater. 5 (2022) 024001 https://doi.org/10.1088/2399-7532/ac55fd

Multifunctional Materials

OPEN ACCESS

RECEIVED
25 January 2022

ACCEPTED FOR PUBLICATION
16 February 2022

PUBLISHED
29 March 2022

PAPER

Optically controlled grasping-slipping robot moving on tubular surfaces

Hongshuang Guo*, Hao Zeng and Arri Priimagi*

Smart Photonic Materials, Faculty of Engineering and Natural Sciences, Tampere University, P.O. Box 541, FI-33101 Tampere, Finland
* Authors to whom any correspondence should be addressed.

E-mail: hongshuang.guo@tuni.fi **and** arri.priimagi@tuni.fi

Keywords: photoactuation, liquid crystal elastomer, soft robot, controllable friction

Supplementary material for this article is available online

Abstract

Stimuli-responsive polymers provide unmatched opportunities for remotely controlled soft robots navigating in complex environments. Many of the responsive-material-based soft robots can walk on open surfaces, with movement directionality dictated by the friction anisotropy at the robot-substrate interface. Translocation in one-dimensional space such as on a tubular surface is much more challenging due to the lack of efficient friction control strategies. Such strategies could in long term provide novel application prospects in, e.g. overhaul at high altitudes and robotic operation within confined environments. In this work, we realize a liquid-crystal-elastomer-based soft robot that can move on a tubular surface through optical control over the grasping force exerted on the surface. Photoactuation allows for remotely switched gripping and friction control which, together with cyclic body deformation, enables light-fueled climbing on tubular surfaces of glass, wood, metal, and plastic with various cross-sections. We demonstrate vertical climbing, moving obstacles along the path, and load-carrying ability (at least 3 × body weight). We believe our design offer new prospects for wirelessly driven soft micro-robotics in confined spacing.

1. Introduction

Soft robotics is a hot topic in contemporary science and technology, due to potential opportunities in, e.g. industrial manufacturing and medical treatments [1–5]. Distinct from conventional hard-bodied machines, soft robots can adopt flexible material composition, possess high degrees of freedom in body deformation, and they can adjust when meeting irregular hurdles or unexpected environments [6–10]. Due to the flexibility and adaptivity [11], soft robots are foreseen to provide novel opportunities in human interfacing, space exploration and task execution in complex medical environments [9, 12]. For potential applications in *in-vivo* biomedical settings [13, 14], pneumatic [15, 16] and dielectric [17, 18] actuators are too bulky, and they usually require wire connections. To address this challenge, an attractive alternative is to use stimuli-responsive materials for actuation, while powering the system remotely. Several stimuli-responsive materials have been developed for soft robotics, including thermally driven bilayers [19, 20], magnetically driven systems [21, 22], ion-driven hydrogels [23], humidity-driven films [24, 25], and light-driven liquid crystal elastomers (LCEs) [26–29]. In particular, the light-driven LCEs offer a solid material framework for building high-performance actuating robotic materials, as their movement can be precisely spatio-temporally programmed [28, 30]. Based on these materials, various soft robots in the open space environment have been prepared, including walking [31], rolling [32–34], crawling [35], jumping [36], and swimming robots [37–39].

One of the mainstreams of responsive-material-based soft robotics is to mimic the movement of animals [4] or plants [40], in order to simplistically capture their elementary principles to realize functions such as grasping objects and controlled locomotion [28, 41–43]. Considering a soft micro-object moving on a 2D surface, the body of the object must cyclically change, while asymmetric structure and friction control

[44, 45] are needed for locomotion directionality [46, 47]. Locomotion in linear spaces like on a tubular surface [48, 49], is also important, potentially opening up opportunities for robotic operation on power lines, fiber-optic cables and other narrowly confined environments. In the far future, a responsive-material-based soft robot crawling in confined environments to excurse the installation, cleaning, testing and repairing without human intervention, could increase the efficiency and minimize the cost of operations [48]. Realizing a soft robot navigating on tubular surfaces requires a strategy to control the friction, and sufficient mechanical strength to overcome gravity [49], which is challenging especially for small-sized robots with limited degrees of freedom of deformation. Only few reports about robotic movement in tubular environments exist [50], most of them relying on wire or tube connections [51, 52]. Wireless robots would in this context have the obvious benefit of increased freedom of mobility [53].

In this work, we demonstrate a light-driven soft robot that can move on tubular surfaces. The robot is made of optically deformable LCE, composed of two semi-circular grippers at both ends for position fixation and a bending body for inducing the mass translocation. The two grippers are optically controlled to open and close alternately, and the cyclic bending of the body is transformed into translocation toward the manually dictated direction. The robot can move on plastic, wood, metal, and glass surfaces, and climb on a vertically placed tube. We also demonstrate functions such as removing an obstacle and cargo transport of 3 times the robot's body weight.

2. Results and discussion

2.1. Soft robot design

In nature, many tree-climbing animals may serve as good textbook-type inspiration for soft robotics. One example is shown in figure 1(a), where a monkey is holding a tree trunk through the closure of its arms. When starting to climb, it tightens its hands and unlocks the legs to move them upward. Then, it locks the legs and loosens the hands to lift up the body mass. By repeating this action, the monkey is able to translocate on the tree trunk. In this process, the critical points from the perspective of robotics are (1) change of arm and leg curvature, allowing control over the friction between the animal and the trunk, and (2) large body deformation, providing the mass translocation.

Our soft robot design is based on a chain-extended LCE with a bending body and two gripping segments, as shown in figures 1(b) and (c). Both the body and the gripping segments are light-responsive, and their chemical composition is shown in figure 1(d) (see figure S1 and Materials and Methods for preparation details available online at stacks.iop.org/MFM/5/024001/mmedia). The chain-extended LCE combines large deformability, facile control over molecular alignment, and versatile deformation modes [54, 55]. We employ splay alignment to enable large-magnitude and reversible light-induced bending upon photothermal heating (figures 1(c) and S2) [56–58]. Disperse Red 1, a light-absorbing dye, was incorporated into the elastomer to yield the photothermal heat generation for material actuation (see figure S3 for absorption spectrum) [30]. Different from photochemical actuation that is caused by cis-trans isomerization of azobenzene crosslinks, photothermal actuation results from heat-induced disorder and resultant strains within the initially ordered polymer network. The main difference between these two actuation mechanisms relates to the actuation speed, which is much faster for the latter. Systematic characterization of the LCE actuator used, in terms of reversible light-induced bending, the tip displacement upon forward and reverse bending, and response time, are given in figure S4, while figure S5 reveals actuation bandwidth of ca. 0.1 Hz at the light intensities used. The young's modulus of the chain-extended LCE (20 MPa) is significantly lower than the modulus of a sample prepared without the chain-extender (1070 MPa), as shown in figure S6. Hence, the chain extension renders LCE significantly more elastic, increasing the deformation strain that can be obtained. The chain-extended LCE can also generate sufficient bending force upon illumination to overcome its own gravity. As shown in figure 1(e), the grippers can open and close, which, combined with the light-induced body deformation, enable controlled robotic movements.

2.2. Light-controlled movement on tubular surfaces

Figure 2(a) shows the translocation mechanism of the robot on a tubular surface. A light beam is scanning along with the robot from head to tail. When the light arrives at the front segment, the paw opens to reduce the friction. When the beam reaches the middle part, the bending body is able to overcome the friction at the front and move the front paw forward. By the time the beam arrives at the back side to unlock the back paw, the front paw re-establishes the fixation with the tubular substrate. Thus, the back paw moves forward when the robot body starts to unbend after ceasing the light. Alternated grasping and slipping movements are induced by light actuation through opening and closure of the paw segments, as indicated by the position tracking in figure 2(b). Repeating the light scanning process yields a continuous mass translocation on the tubular surface. A higher intensity produces a more effective photo-deformation, while a larger strip

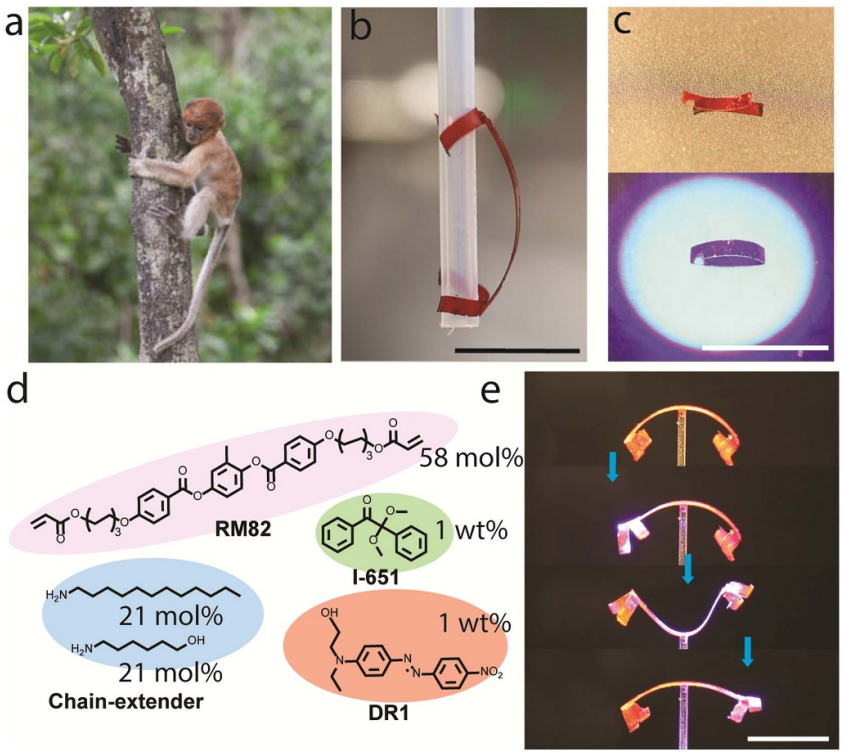

Figure 1. The light-controlled tube-climbing robot. (a) Natural example of a monkey climbing a tree. Credit: Rosanne Tackaberry / Alamy Stock Photo (adapted with permission). (b) Photograph of the light-controlled soft LCE robot on a plastic tube. (c) Splayed LCE actuator in the dark (top) and under light illumination (bottom). (d) Chemical composition of the LCE used. (e) Photographs of the opening/closing and body deformation of the light-controlled robot. All scale bars: 1 cm.

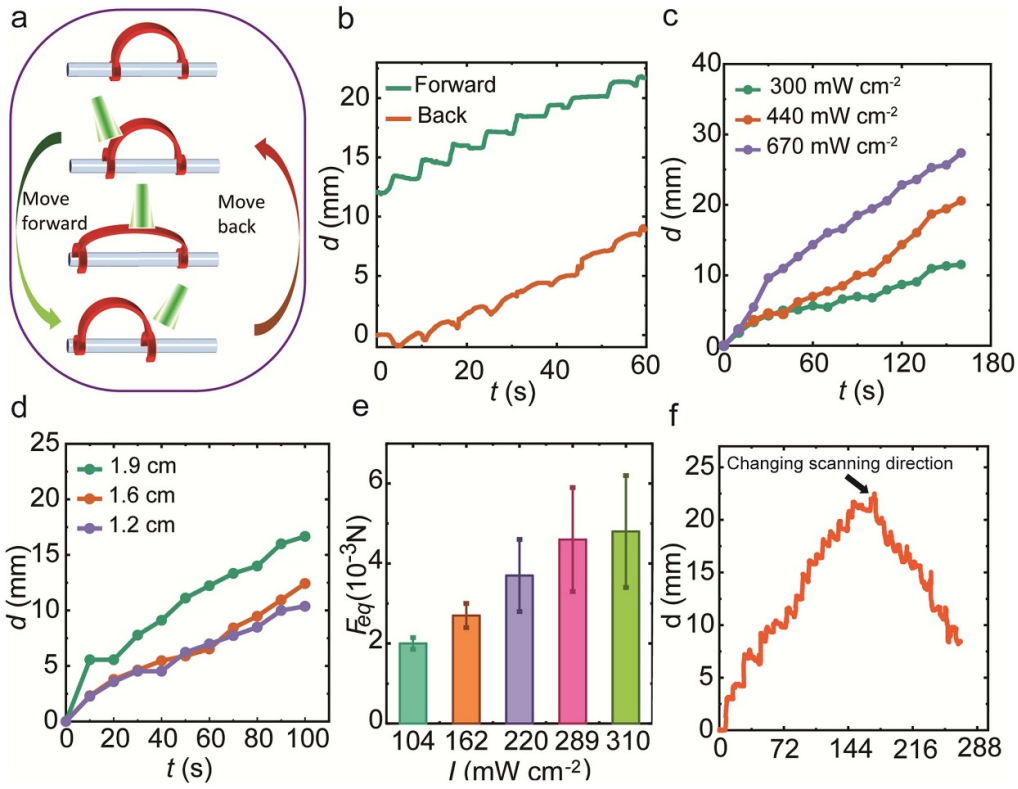

Figure 2. Locomotion characterization. (a) Schematic diagram of the robotic movement. (b) Displacement of the front and back paws along horizontal direction. The power dependence (c) and body-length dependence (d) of the light-induced movement. (e) Light-induced force generation in LCE with different light intensities, and (f) tracking of the mass center during robotic movement. Excitation: 460 nm, 440 mW cm^{-2} (unless otherwise mentioned).

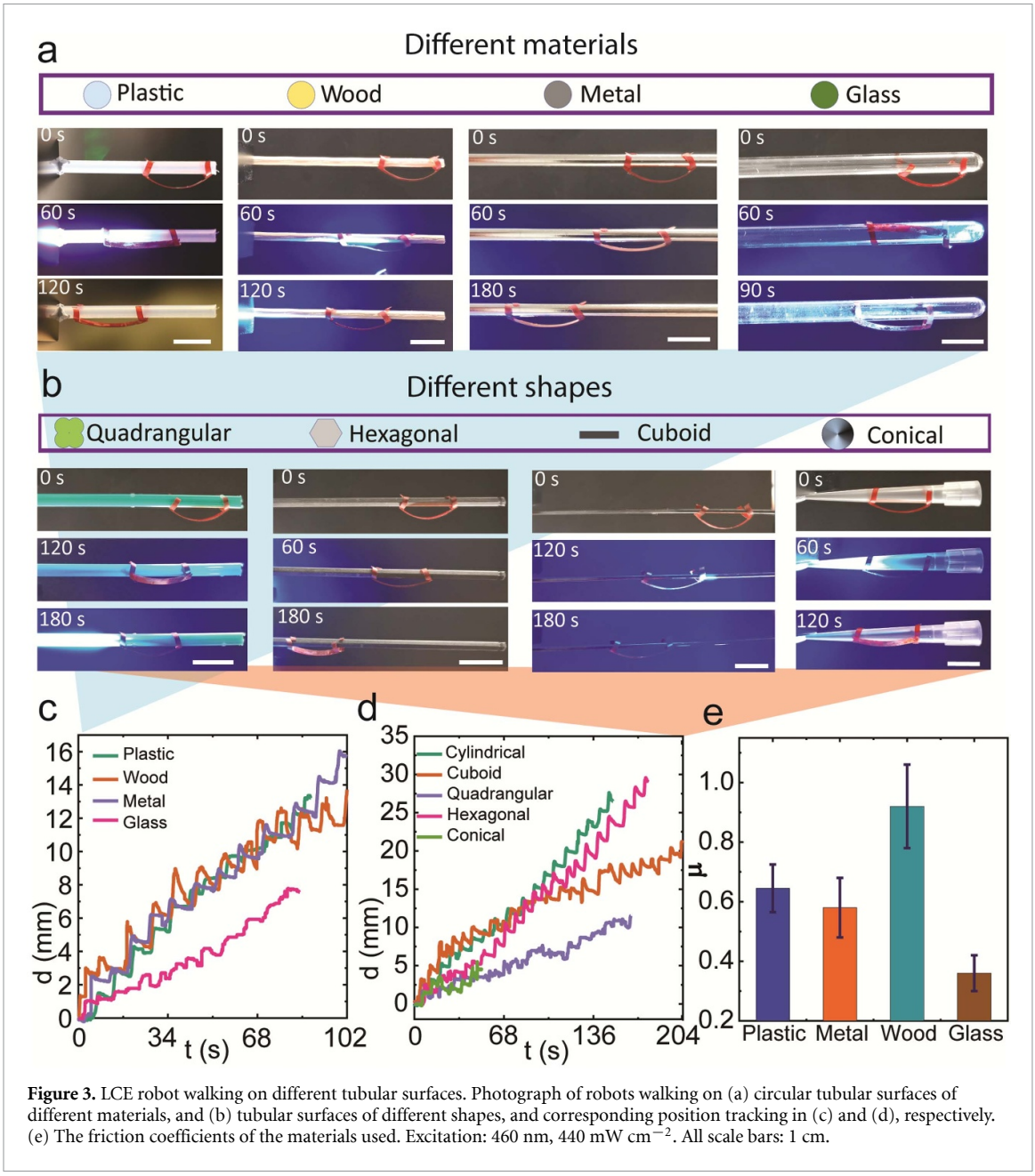

Figure 3. LCE robot walking on different tubular surfaces. Photograph of robots walking on (a) circular tubular surfaces of different materials, and (b) tubular surfaces of different shapes, and corresponding position tracking in (c) and (d), respectively. (e) The friction coefficients of the materials used. Excitation: 460 nm, 440 mW cm^{-2}. All scale bars: 1 cm.

dimension increases the step length, both enhancing the translocation velocity (figures 2(c) and (d)). The bending force produced by the light-controlled paw is about 3 mN (figure S7), and the friction force that can be generated by the bending force on the surface is 10 mN (figure 2(e), see measurement details in figures S7(e) and (f)), sufficient to lift objects weighing 10 mN. This is sufficient to support the robot's body weight (8 mg, 0.1 mN) and induce directional movement on the tubular surface. The energy efficiency was also calculated by measuring the input light energy and the output work, yielding maximum efficiency of 0.0002% (figure S8). As shown in figure 2(f) and video S1, by switching the light scanning direction, the robot can walk to the opposite direction with a similar velocity. Note that the robot does not rely on an asymmetric structure to determine the friction bias, as is the case in most reports [59]. Rather the light-induced deformation provides the friction control, and the walking direction is dictated by the beam scanning direction.

In this work, we have used splay-aligned LCE actuators, which enable reversible light-induced bending [56, 57]. The actuation is driven by the photothermal effect, i.e. temperature increase and resultant disruption of the LCE molecular alignment upon light irradiation. This mechanism always leads to bending towards the side where the molecules are arranged parallel to the surface [28, 60]. Upon reduction of the body length, the robot walks with shorter steps and can hardly move when the length is <0.9 cm. If the body length is too long (*ca.* > 2.0 cm), the robot cannot generate enough bending force to make the robot move, while the

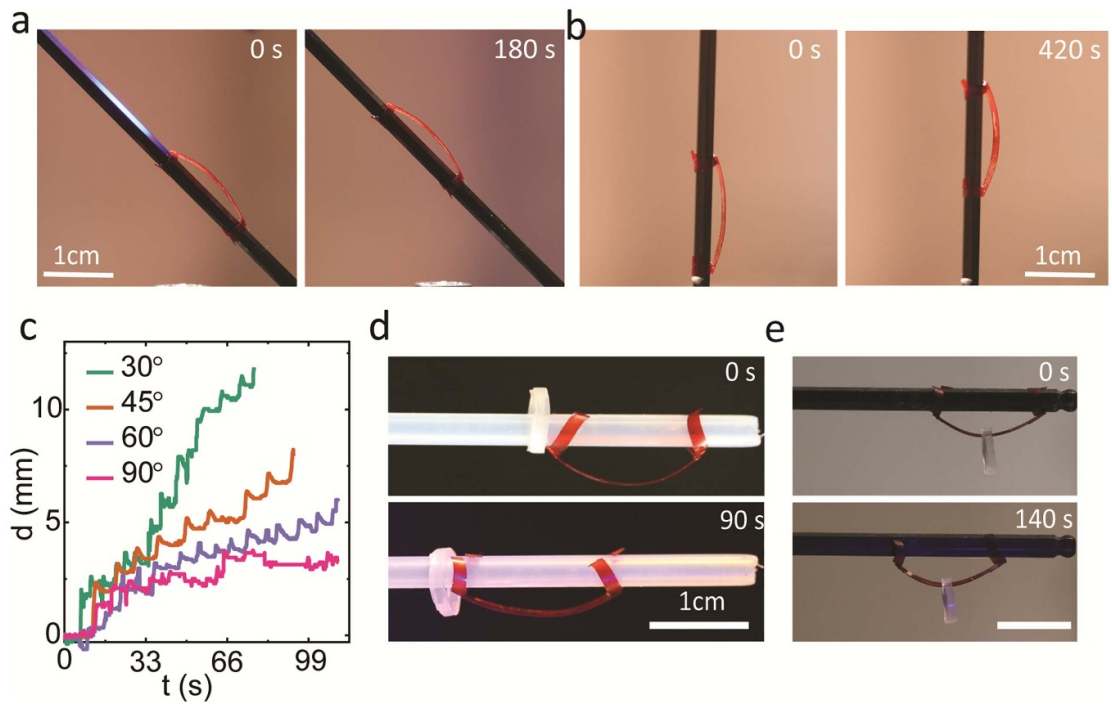

Figure 4. Vertical climbing, obstacle removal, and load-carrying. Photographs of robots moving on a 45° ramp (a) and on a vertical tube (b). (c) Displacement tracking of the robot walking on inclined surfaces. (d) Photograph of a robot walking on a horizontal surface with an obstacle in front of it. (e) Photograph of a robot walking on horizontal surface carrying a load of three times its body weight. Excitation: 460 nm, 440 mW cm^{-2}. All scale bars: 1 cm.

length increases, the frictional force for the movement of the paws increases. Hence there is an optimal body length of about 1.9 cm (figure 2(d)) to maximize the moving speed. In the same way, strong light intensity leads to rapid deformation, giving rise to increased translocation velocity under sequential irradiation cycles.

2.3. Light-controlled robot walking on different tubular surfaces

The surface roughness of the substrate may greatly influence the movement of the robot [45, 61, 62]. Thus, we tested the walking performance on tubular surfaces of plastic, wood, metal, and glass. As shown in figure 3(a), the robot can walk on tubes made of each of these (video S2). The walking distance increases with the light scanning cycles, as shown by the position tracking data in figure 3(c). Details on the size of the robot and the substrate dimensions are given in table S1. The walking velocity is similar for plastic, wood, and metal tubes, and somewhat lower for the glass tube. This is ascribed to the low friction coefficient between LCE and glass (figure 3(e)), decreasing the locking ability of the paw segments, yielding bi-directional slipping during the cyclic body change and reducing the mean translocation velocity. Apart from tubular surfaces with a circular cross-section, we tested the robot on tubes with different shapes. As shown by the snapshots in figure 3(b) and tracking of position in figure 3(d), the robot is capable of walking also on quadrangular, hexagonal (video S3), cuboid and conical substrates.

For the robot to move unidirectionally, the typical design strategy is to increase the friction of the substrate surface [43]. However, in this work, we keep the substrate roughness intact, and the friction between the robot and the substrate surface is purely light-controlled, allowing movement even on (tubular) surfaces with a low friction coefficient. As shown in figures 3(b) and (d), the LCE robot can move on various shapes of tubular surfaces. In case of the tapered tube, however, the gradient in the tube diameter prevents long-distance travel, indicating that for efficient movement to take place, the shape of the tube must fit the gripper so that it can fully grasp it.

2.4. Robot climbing, obstacle removal and load-carrying

The bending force of the robot is measured to be 3 mN, and the friction coefficient of the tubes range from 0.36 (glass) to 0.92 (wood), the effective friction force ($\mu \times$ Fn (bending force)) being 1–2.7 mN. The light-active elastic force is about 3 mN in a $10 \times 2 \times 0.1$ mm^3 -sized strip actuator. Both exceed the gravitational force exerted on the robot, enabling the robot to climb up a ramp. This is demonstrated in figures 4(a), (b) and videos S4, S5 on slopes with 45° and 90° tilt angles, respectively. The movement speed

decreases from 5.0 to 2.4 mm min^{-1} for inclination angles of 45° and 90° (figure 4(c)). This is due to increased slipping tendency caused by gravitation, as shown by positional tracking given in figure S9.

The photoactivated elastic force of the LCE allows the robot to remove obstacles along its path on the tubular surface. The obstacle removal is shown in figure 4(d) and video S6, for an LCE with a mass of 8 mg (obstacle mass: 24 mg). The original walking speed of 10.0 mm min^{-1} reduces to 6.0 mm min^{-1} during the obstacle removal. Figure 4(e) and video S7 demonstrate the load-carrying capacity of the light-fueled LCE robot. A 24 mg load, 3 times the robot's body weight, is attached to the robot body. Under such conditions, the robot can still translocate along the tubular surface, but with velocity decreased from 10.0 mm min^{-1} to 2.1 mm min^{-1}. The difference between the load-carrying and obstacle removal speeds is presumably because when the object is placed in the front, the robot needs to overcome only the friction between the obstacle and the tubular surface, which is far less than the force required by the robot to actually carry the obstacle.

3. Conclusion

We report on a light-driven soft robot that can move on tubular surfaces of different materials and cross-sectional geometries. The light-induced deformation enables geometric switching of the paw segments for locking and unlocking the friction, while bending of the robot body enables alternated step movement to induce translocation. The robot locomotes on tilted and even vertical tubes, removes obstacles along its movement path, and carries a load at least three times its own body weight during the light-fueled movement. The results provide a facile fabrication of soft robots that are suitable for light-driven locomotion within linear space, providing new alternatives for untethered, soft small-scale actuators.

4. Materials and methods

4.1. Materials and LCE film fabrication

The crosslinker 1,4-Bis-[4-(6-acryloyloxyhexyloxy)benzoyloxy]-2-methylbenzene (99%, RM82) was obtained from Synthon Chemicals. 6-Amino-1-hexanol and dodecylamine were obtained from Tokyo Chemical Industry (TCI). 2,2-dimethoxy-2-phenylacetophenone was obtained from Sigma Aldrich. Disperse Red 1 was obtained from Merck. All chemicals were used as received. First, a liquid crystal cell is prepared by taking two pieces of clean glass (sonication in acetone), spin-coated one of them with PI, baking at 100 °C for 10 min and at 180 °C for 30 min to obtain homeotropic LC alignment. The other glass was spin-coated with a 5% polyvinyl alcohol (PVA) solution and baked at 100 °C for 10 min, followed by rubbing with a velvet fabric to obtain a planar LC alignment. Then the two pieces were glued together with UV glue using 100 μm spacers. The liquid crystal mixture to be infiltrated into the liquid crystal cell contains 0.28 mmol RM82, 0.1 mmol 6-Amino-1-hexanol and 0.1 mmol dodecylamine, together with 1 wt % of the total LC mixture photoinitiator (2,2-dimethoxy-2-phenylacetophenone). The mixture was then heated to 80 °C (in the dark) and vigorously vortexed for uniform mixing. After stirring the mixture was infiltrated into the aligned LC cell by capillary action at 80 °C, followed by slow cooling to 63 °C. The LC cell was placed in an oven for approximately 24 h at the temperature of the nematic phase (63 °C) for each mixture, which allowed aza-Michael addition reaction between diacrylate and amine resulting in step-growth oligomerization. Then, the sample was photopolymerized with UV light (365 nm, 180 Mw cm^{-2}, 30 min) at 50 °C for photopolymerization of diacrylate (the polymerization temperature of the arcs is 63 °C), after which the cell was opened and samples of proper size cut from the LCE film. Before cutting the sample, we need to diffuse the Disperse Red 1 into the LCE film for later use. First to put the sample (25 × 25 mm^2) on a 110 °C hot plate, and then spread 1 mg of Disperse Red 1 on the sample surface. Then, the sample is put on 110 °C hot plate for about 5 min to ensure sufficient dye diffusion. The residual dye on the surface is removed by a cotton swab containing acetone.

4.2. Fabrication and characterization of the LCE robot

Optical images and movies were recorded by using a Canon 5D Mark III camera equipped with a 100 mm objective. A LED source (CoolLED pE-4000) was used for light-induced deformation. A force sensor (F329, Novatech, resolution 4 μN) was used to measure the bending force. To fabricate the LCE robot, the photopolymerized film was first to cut into strips of different lengths. Then, two curved arcs (length 12 mm, width 2 mm, thickness 0.1 mm, because the polymerization temperature is 63 °C, the sample in room temperature will bend to the side where the molecules are arranged homeotropic, see in figure 1(e)) were picked and glued to the ends of the strip playing the role of the robot body (length 12, 16 or 19 mm, width 2 mm and thickness 0.1 mm). The movement of the LCE robot was controlled by manually scanning the light (wavelength, power range) over the robot, at a distance of about 1 cm. The movement was recorded and quantitative data were extracted from the movie with a video analysis software (kinovea).

Data availability statement

The data that support the findings of this study are available upon reasonable request from the authors.

Acknowledgments

We acknowledge the financial support of the Academy of Finland, provided through an Academy project P-Cap (No. 324353), an Academy Research Fellowship project FAIRY (No. 340263), the Flagship Programme on Photonics Research and Innovation (PREIN, No. 320165), and the Centre of Excellence on Life-Inspired Hybrid Materials Research (LIBER, No. 346107).

Conflict of interest

There are no conflicts to declare.

ORCID iDs

Hongshuang Guo https://orcid.org/0000-0003-3503-1774
Hao Zeng https://orcid.org/0000-0002-9150-214X
Arri Priimagi https://orcid.org/0000-0002-5945-9671

References

[1] Rus D and Tolley M T 2015 Design, fabrication and control of soft robots *Nature* **521** 467
[2] Trimmer B 2013 Soft robots *Curr. Biol.* **23** R639
[3] Hod L 2014 Challenges and opportunities for design, simulation, and fabrication of soft robots *Soft Robot.* **1** 21
[4] Wehner M, Truby R L, Fitzgerald D J, Mosadegh B, Whitesides G M, Lewis J A and Wood R J 2016 An integrated design and fabrication strategy for entirely soft, autonomous robots *Nature* **536** 451
[5] Jørgensen J, Bojesen K B and Jochum E 2022 Is a soft robot more 'natural'? Exploring the perception of soft robotics in human–robot interaction *Int. J. Soc. Robot.* **14** 95
[6] Shah D S, Powers J P, Tilton L G, Kriegman S, Bongard J and Kramer-Bottiglio R 2021 A soft robot that adapts to environments through shape change *Nat. Mach. Intell.* **3** 51
[7] Zhang B, Fan Y, Yang P, Cao T and Liao H 2019 Worm-like soft robot for complicated tubular environments *Soft Robot.* **6** 399
[8] Fan J, Wang S, Yu Q and Zhu Y 2020 Swimming performance of the frog-inspired soft robot *Soft Robot.* **7** 615
[9] Lee C, Kim M, Kim Y J, Hong N, Ryu S, Kim H J and Kim S 2017 Soft robot review *Int. J. Control Autom. Syst.* **15** 3
[10] Wang H, Totaro M and Beccai L 2018 Toward perceptive soft robots: progress and challenges *Adv. Sci.* **5** 1800541
[11] Lancia F, Ryabchun A, Nguindjel A-D, Kwangmettatam S and Katsonis N 2019 Mechanical adaptability of artificial muscles from nanoscale molecular action *Nat. Commun.* **10** 4819
[12] Kim Y, Parada G A, Liu S and Zhao X 2019 Ferromagnetic soft continuum robots *Sci. Robot.* **4** eaax7329
[13] Sitti M 2018 Miniature soft robots—road to the clinic *Nat. Rev. Mater.* **3** 74
[14] Hines L, Petersen K, Lum G Z and Sitti M 2017 Soft actuators for small-scale robotics *Adv. Mater.* **29** 1603483
[15] Drotman D, Jadhav S, Sharp D, Chan C and Tolley M T 2021 Electronics-free pneumatic circuits for controlling soft-legged robots *Sci. Robot.* **6** eaay2627
[16] Whitesides G M 2018 Soft robotics *Angew. Chem., Int. Ed.* **57** 4258
[17] Ji X, Liu X, Cacucciolo V, Imboden M, Civet Y, Haitami A E, Cantin S, Perriard Y and Shea H 2019 An autonomous untethered fast soft robotic insect driven by low-voltage dielectric elastomer actuators *Sci. Robot.* **4** eaaz6451
[18] Acome E, Mitchell S K, Morrissey T G, Emmett M B, Benjamin C, King M, Radakovitz M and Keplinger C 2018 Hydraulically amplified self-healing electrostatic actuators with muscle-like performance *Science* **359** 61
[19] Tang Z, Gao Z, Jia S, Wang F and Wang Y 2017 Graphene-based polymer bilayers with superior light-driven properties for remote construction of 3D structures *Adv. Sci.* **4** 1600437
[20] Gao G, Wang L, Cong Y, Wang Z, Zhou Y, Wang R, Chen J and Fu J 2018 Synergistic pH and temperature-driven actuation of poly(NIPAM-co-DMAPMA)/clay nanocomposite hydrogel bilayers *ACS Omega* **3** 17914
[21] Hu W, Lum G Z, Mastrangeli M and Sitti M 2018 Small-scale soft-bodied robot with multimodal locomotion *Nature* **554** 81
[22] Ren Z, Hu W, Dong X and Sitti M 2019 Multi-functional soft-bodied jellyfish-like swimming *Nat. Commun.* **10** 2703
[23] Hua M, Kim C, Du Y, Wu D, Bai R and He X 2021 Swaying gel: chemo-mechanical self-oscillation based on dynamic buckling *Matter* **4** 1029
[24] Lv C, Xia H, Shi Q, Wang G, Wang Y-S, Chen Q-D, Zhang Y-L, Liu L-Q and Sun H-B 2017 Sensitively humidity-driven actuator based on photopolymerizable PEG-DA films *Adv. Mater. Interfaces* **4** 1601002
[25] Castaldo R, Lama G C, Aprea P, Gentile G, Ambrogi V, Lavorgna M and Cerruti P 2019 Humidity-driven mechanical and electrical response of graphene/cloisite hybrid films *Adv. Funct. Mater.* **29** 1807744
[26] Wani O M, Zeng H and Priimagi A 2017 A light-driven artificial flytrap *Nat. Commun.* **8** 15546
[27] Dong L and Zhao Y 2018 Photothermally driven liquid crystal polymer actuators *Mater. Chem. Front.* **2** 1932
[28] Da Cunha M P, Debije M G and Schenning A P 2020 Bioinspired light-driven soft robots based on liquid crystal polymers *Chem. Soc. Rev.* **49** 6568
[29] Ge F, Yang R, Tong X, Camerel F and Zhao Y 2018 A multifunctional dye-doped liquid crystal polymer actuator: light-guided transportation, turning in locomotion, and autonomous motion *Angew. Chem., Int. Ed.* **57** 11758
[30] Gelebart A H, Jan Mulder D, Varga M, Konya A, Vantomme G, Meijer E W, Selinger R L B and Broer D J 2017 Making waves in a photoactive polymer film *Nature* **546** 632

[31] Xiao Y-Y, Jiang Z-C, Tong X and Zhao Y 2019 Biomimetic locomotion of electrically powered 'janus' soft robots using a liquid crystal polymer *Adv. Mater.* **31** 1903452
[32] Lu X, Guo S, Tong X, Xia H and Zhao Y 2017 Tunable photocontrolled motions using stored strain energy in malleable azobenzene liquid crystalline polymer actuators *Adv. Mater.* **29** 1606467
[33] Wie J J, Shankar M R and White T J 2016 Photomotility of polymers *Nat. Commun.* **7** 13260
[34] Cheng Y-C, Lu H-C, Lee X, Zeng H and Priimagi A 2020 Kirigami-based light-induced shape-morphing and locomotion *Adv. Mater.* **32** 1906233
[35] Sun Z, Yamauchi Y, Araoka F, Kim Y S, Bergueiro J, Ishida Y, Ebina Y, Sasaki T, Hikima T and Aida T 2018 An anisotropic hydrogel actuator enabling earthworm-like directed peristaltic crawling *Angew. Chem., Int. Ed.* **57** 15772
[36] Ahn C, Liang X and Cai S 2019 Bioinspired design of light-powered crawling, squeezing, and jumping untethered soft robot *Adv. Mater. Technol.* **4** 1900185
[37] Zhao Y, Xuan C, Qian X, Alsaid Y, Hua M, Jin L and He X 2019 Soft phototactic swimmer based on self-sustained hydrogel oscillator *Sci. Robot.* **4** eaax7112
[38] Shahsavan H, Aghakhani A, Zeng H, Guo Y, Davidson Z S, Priimagi A and Sitti M 2020 Bioinspired underwater locomotion of light-driven liquid crystal gels *Proc. Natl Acad. Sci. USA* **117** 5125
[39] Palagi S *et al* 2016 Structured light enables biomimetic swimming and versatile locomotion of photoresponsive soft microrobots *Nat. Mater.* **15** 647
[40] Esser F J, Auth P and Speck T 2020 Artificial venus flytraps: a research review and outlook on their importance for novel bioinspired materials systems *Front. Robot. AI* **7** 75
[41] Yoon C 2019 Advances in biomimetic stimuli responsive soft grippers *Nano Converg.* **6** 20
[42] Ng C S X, Tan M W M, Xu C, Yang Z, Lee P S and Lum G Z 2021 Locomotion of miniature soft robots *Adv. Mater.* **33** 2003558
[43] Qian X *et al* 2019 Artificial phototropism for omnidirectional tracking and harvesting of light *Nat. Nanotechnol.* **14** 1048
[44] Xiao Y-Y, Jiang Z-C and Zhao Y 2020 Liquid crystal polymer-based soft robots *Adv. Intell. Syst.* **2** 2000148
[45] Manoonpong P, Petersen D, Kovalev A, Wörgötter F, Gorb S N, Spinner M and Heepe L 2016 Enhanced locomotion efficiency of a bio-inspired walking robot using contact surfaces with frictional anisotropy *Sci. Rep.* **6** 39455
[46] Xu T, Zhang J, Salehizadeh M, Onaizah O and Diller E 2019 Millimeter-scale flexible robots with programmable three-dimensional magnetization and motions *Sci. Robot.* **4** eaav4494
[47] Zeng H, Wani O M, Wasylczyk P and Priimagi A 2018 Light-driven, caterpillar-inspired miniature inching robot *Macromol. Rapid Commun.* **39** 1700224
[48] Chu B, Jung K, Han C-S and Hong D 2010 A survey of climbing robots: locomotion and adhesion *Int. J. Precis. Eng. Man.* **11** 633
[49] Lam T L and Xu Y 2012 Biologically inspired tree-climbing robot with continuum maneuvering mechanism *J. Field Robot.* **29** 843
[50] Cheng M, Zeng H, Li Y, Liu J, Luo D, Priimagi A and Liu Y J 2021 Light-fueled polymer film capable of directional crawling, friction-controlled climbing, and self-sustained motion on a human hair *Adv. Sci.* **9** 2103090
[51] Liao B, Zang H, Chen M, Wang Y, Lang X, Zhu N, Yang Z and Yi Y 2020 Soft rod-climbing robot inspired by winding locomotion of snake *Soft Robot.* **7** 500
[52] Verma M S, Ainla A, Yang D, Harburg D and Whitesides G M 2018 A soft tube-climbing robot *Soft Robot.* **5** 133
[53] Son D, Ugurlu M C and Sitti M 2021 Permanent magnet array-driven navigation of wireless millirobots inside soft tissues *Sci. Adv.* **7** eabi8932
[54] Yoon H-H, Kim D-Y, Jeong K-U and Ahn S-K 2018 Surface aligned main-chain liquid crystalline elastomers: tailored properties by the choice of amine chain extenders *Macromolecules* **51** 1141
[55] Ware T H, McConney M E, Wie J J, Tondiglia V P and White T J 2015 Voxelated liquid crystal elastomers *Science* **347** 982
[56] Pang X, Lv J A, Zhu C, Qin L and Yu Y 2019 Photodeformable azobenzene-containing liquid crystal polymers and soft actuators *Adv. Mater.* **31** 1904224
[57] Kuenstler A S, Chen Y, Bui P, Kim H, DeSimone A, Jin L and Hayward R C 2020 Blueprinting photothermal shape-morphing of liquid crystal elastomers *Adv. Mater.* **32** 2000609
[58] Mol G N, Harris K D, Bastiaansen C W M and Broer D J 2005 Thermo-mechanical responses of liquid-crystal networks with a splayed molecular organization *Adv. Funct. Mater.* **15** 1155
[59] Lu X, Zhang H, Fei G, Yu B, Tong X, Xia H and Zhao Y 2018 Liquid-crystalline dynamic networks doped with gold nanorods showing enhanced photocontrol of actuation *Adv. Mater.* **30** 1706597
[60] White T J and Broer D J 2015 Programmable and adaptive mechanics with liquid crystal polymer networks and elastomers *Nat. Mater.* **14** 1087
[61] Tramsen H T, Heepe L, Homchanthanakul J, Wörgötter F, Gorb S N and Manoonpong P 2021 Getting grip in changing environments: the effect of friction anisotropy inversion on robot locomotion *Appl. Phys.* A **127** 389
[62] Shen T, Font M G, Jung S, Gabriel M L, Stoykovich M P and Vernerey F J 2017 Remotely triggered locomotion of hydrogel mag-bots in confined spaces *Sci. Rep.* **7** 1